Novel Method for the Modeling and Control Investigation of Efficient Swimming for Robotic Fish

Li Wen, Tianmiao Wang, Guanhao Wu, Jianhong Liang, and Chaolei Wang

***Abstract*—In this paper, analytical techniques and fuzzy logic method are applied to the dynamic modeling and efficient swimming control of a robotic fish. The bioinspired robotic fish, which follows an exact replica of a live mackerel (*Scomber scombrus*), is modeled by treating the undulating body and flapping tail independently using analytical methods. Comparing the results of simulations and experiments shows the feasibility of the dynamic model. Using this model, we found that the harmonic control of the Strouhal number and caudal fin angle of attack is a principal mechanism through which the robotic fish can obtain high thrust efficiency while swimming. The fuzzy control method, which is based on the knowledge of the robotic fish's dynamic behavior, has successfully utilized this principal mechanism. By comparing the thrust performance of the robotic fish with different control methods via simulation, we established that the fuzzy controller was able to achieve faster acceleration and smaller steady-state error than what could be achieved from an open-loop and conventional proportional–integral-derivative controller. The thrust efficiency during steady state was superior to that with conventional control methods. We also found that, when using the fuzzy control method, robotic fish can always swim near a "universal" Strouhal number that approximates to the swimming of live fish.**

***Index Terms*—Fuzzy control, robotic fish, thrust efficiency, vorticity control.**

I. Introduction

THROUGH bionic engineering, the high thrust performance of fish has been used to compensate for the defects in traditional underwater vehicles, particularly low efficiency. Several previous researchers have provided evidence that live fish movements are efficient [1]. These movement patterns are mostly described using dimensionless parameters by many comparative biology [2] or biomechanics researchers. The optimal swimming pattern for robotic fish needs to be seriously considered. Man-made robotic swimmers have inherent characteristics such as skin friction and body flexibility and form which obviously vary from those of live swimming fish [3]. Therefore, the simple application of the biological observed data to the control of robotic fish would lead to an imperfect result of the thrust performance [4], [6]. The current research presented here aims to investigate how biomimetic robotic fish can swim efficiently in water. The robotic fish which we chose to investigate in this paper belongs to the group exhibiting the body and/or caudal fin movement pattern [7]. Existing prior research relevant to the materials presented here, and current contributions, can be broadly classified into two categories: dynamic modeling of and control methods for robotic fish.

A. Dynamic Modeling

In conventional studies on carangiform robotic fish, the body and tail are treated together as a single flexible undulating curve [7], [8]. However, observation results have shown that the caudal fin of fish undergoes different slope angles and moves independently of the body undulations [9]. Biologists also suggested that undulating swimming of carangiform fish should be conceptualized as the movement of a waving plate and an independent flapping foil [10], where the caudal fin corresponds to the downstream flapping foil and the undulating body denotes the upstream waving plate, both of which influence the thrust performance of robotic fish [11]. Considering the analytical approach for the dynamic modeling of the undulating body thrust, the large-amplitude elongated-body theory (LAEBT) [12] was used to provide a dynamic model for a number of planar or 3-D motions of robotic fish under inviscid conditions [13], [14]. While considering the caudal fin thrust, the dynamics of the flapping foil under the assumption of 2-D ideal flow was applied to the caudal fin force modeling [15], [16], and this analytical method, based on the linear foil theory, was applied to several dynamic modeling studies of fin-actuated systems [17].

In this paper, we mimic a typical carangiform fish, mackerel (*Scomber scombrus*), whose morphological data have been adequately provided [18], and its swimming dynamics are computed by treating the thrust force of the body and caudal fin separately. Moreover, the hydrodynamic function of the median fin (i.e., dorsal and pelvic fins) is also taken into consideration. To validate the feasibility of the dynamic model, although a variety of different free swimming autonomous robotic fish designs

Manuscript received April 6, 2010; revised October 15, 2010 and March 17, 2011; accepted April 20, 2011. Date of publication May 5, 2011; date of current version March 30, 2012. This work was supported by the National Science Foundation support projects, China, under Contract 61075100.

L. Wen is with Department of Organismic and Evolutionary Biology, Harvard University, Cambridge, MA 02138 USA (e-mail: liwen@oeb.harvard.edu).

T. Wang, J. Liang, and C. Wang are with the Institute of Robotics, School of Mechanical Engineering and Automation, Beihang University, Beijing 100083, China (e-mail: wtm_itm@263.net; dommy_leung@263.net; chaoleiwang@163.com).

G. Wu is with the State Key Laboratory of Precision Measurement Technology and Instruments, Department of Precision Instruments and Mechanology, Tsinghua University, Beijing 100084, China (e-mail: tophow99@mails.tsinghua.edu.cn).

Color versions of one or more of the figures in this paper are available online at http://ieeexplore.ieee.org.

Digital Object Identifier 10.1109/TIE.2011.2151812

have been produced [5], [19]–[21], systematic experiments for testing dynamic performance can only be conducted using a laboratory model that allows specific movement patterns and certain quantitative measurements to be carried out. In our previous experimental work, we introduced a novel method for the hydrodynamic testing of robotic fish [22], and in this paper, simulation results will be compared with the experimental data to validate the feasibility of the dynamic model.

B. Control Methods

When applied to the control of robotic fish, previous research on motion control mainly focused on the open-loop method for swimming gait generation and closed-loop control based on the dynamic model. The open-loop method usually applied discrete mechanical multilink movements to fit the continuous body curve [23]–[25] or adopted the central pattern generator method to directly generate the sinusoidal signal for the joints [26]. Recently, an alternative approach, using artificial muscles and producing bending deformations to simulate the soft actuation of fish locomotion [27], has frequently been used. However, the open-loop control method can neither help the robotic fish to achieve the desired speed nor obtain high swimming efficiency since there is no speed feedback. Model-based closed-loop control generally uses analytical methods based on the fluid effect to estimate the state of the robotic fish, which also allows control investigation such as trajectory tracking and maneuvering control to be carried out [13], [28]. Furthermore, the fuzzy control method has been credited in various applications as a powerful tool capable of providing controllers for uncertainties and systems with nonlinear dynamics [29]–[32]. This has recently been applied to the control of the tail-fin and pectoral-fin biomimetic systems [8], [33], and the results suggest that fuzzy logic control is highly suitable for the motion control of robotic fish. However, these control methods do not take thrust efficiency, which is the most important metric for the swimming performance of a robotic fish, into consideration. It should be noted that thrust efficiency is one of the most attractive aspects of fish biomimetics.

Considering the merits and shortcomings of previous control methods for making robotic fish swim efficiently and controllably, in this study, we propose to implement a fuzzy control method based on hydrodynamic knowledge to make robotic fish swim efficiently. The results are compared with those of the classical proportional–integral-derivative (PID) controller and the open-loop method.

II. Robotic Fish Design and Experimental Devices

This section provides a brief introduction to robotic fish design. Fig. 1 shows a series of body cross sections for a robotic carangiform swimmer, in three dimensions. It is noted that the change in sharpness of the upper and lower body margins is not obvious. The swimmer has two dorsal fins and two pelvic fins (i.e., the median fins), which are located posterior to the center of mass. The cross section is divided into four regions: 1) mechanical belts and wheels with bearings which play the role of the fish "backbone"; 2) foams and other flexible materials play the role of "muscles;" 3) silica which mimics the "skin;" and 4) median fins.

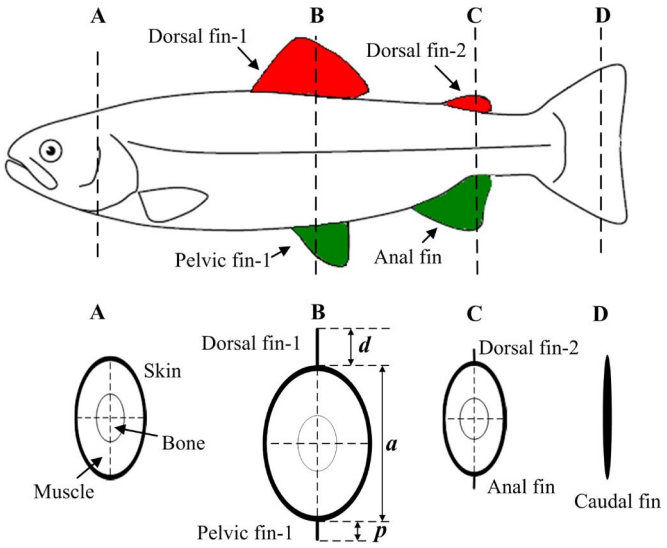

Fig. 1. "Anatomy" of a robotic fish, where clear images of the cross-sectional views are shown.

The robotic fish experimental model has a total length of 0.59 m and consists of a streamlined main body capable of flexing and a rigid caudal fin. The outer shape of the robotic fish is an exact replica of a mackerel, which is a typical carangiform swimmer whose body shape parameters have been adequately modeled [23]. A waterproof outer skin is used to envelop the whole multilink mechanical skeleton to produce a smooth shape, which is capable of fishlike undulation with a form fitting curve, as can be seen in Fig. 2(a). The caudal fin is assumed to have the section shape of the NACA 0012, and the cross section of the body closely resembles an ellipsoidal shape (see Fig. 1 for details). All the robotic fish body parameters are listed in Table I. Fig. 2(b) shows more details of the implementation. The internal mechanism is a high-precision assembly of four anodized aluminum links and is covered by foams and a special structure made of silica. Each mechanical link is capable of rotation with respect to its neighboring links through activation of four brush servomotors. As shown in Fig. 2(c), a belt transmits the motion to individual links with minimal frictional forces.

Fig. 2(d) shows the mechanical components of the test apparatus, where the robotic fish and its associated components are fixed under a multicomponent force transducer which is attached to the towing carriage. The external force of the robotic fish is measured using a multicomponent piezoelectric force transducer (Kislter 9254C) which is assembled vertically above the fish. The control unit and power supply for the robotic fish and the laser system and camera used for flow visualization are all mounted on a carriage rest belt-driven on rails which run in the towing direction (the x direction). The water tank, which is 7.8 m $\times$ 1.2 m $\times$ 1.1 m, provides the robotic model with sufficient space to move without being affected by the boundaries on each side. The fish model is also located at middepth in the tank to avoid any interference effects from the free surface and the bottom of the tank. More details about the apparatus implementation can be found in [34].

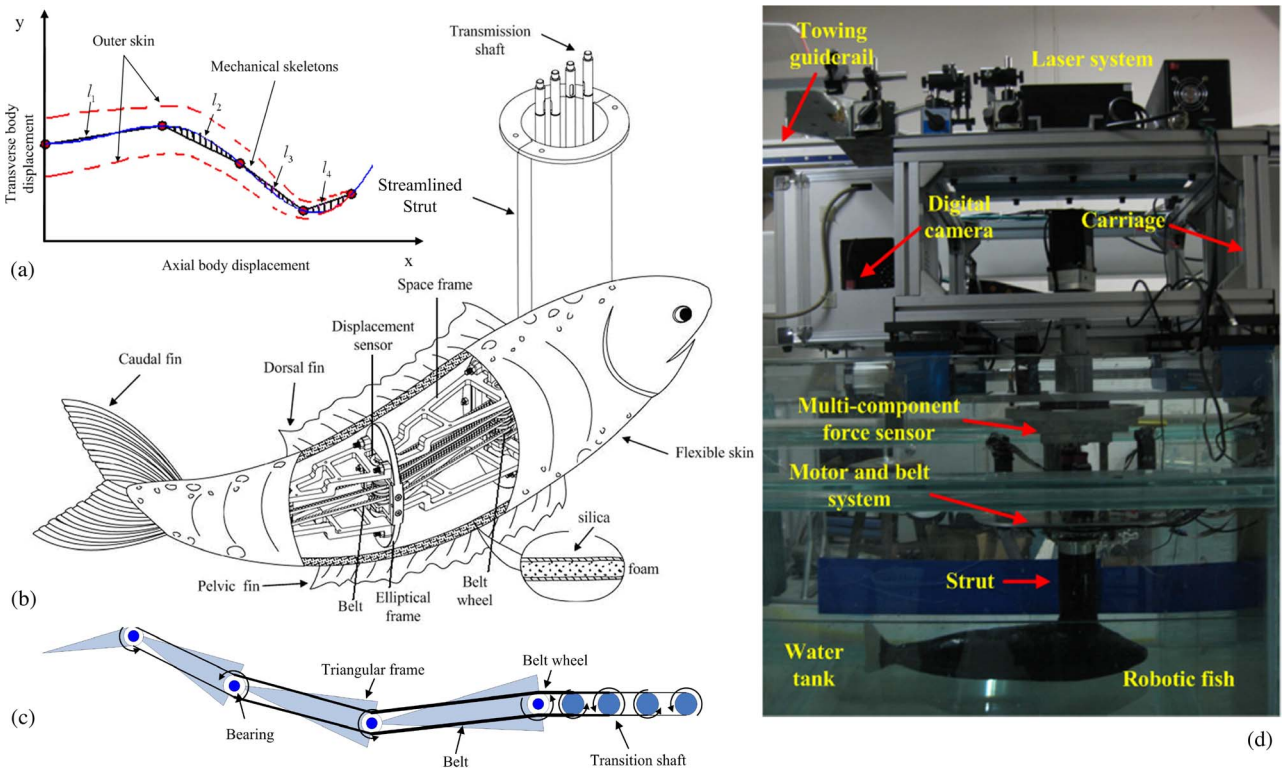

Fig. 2. (a) Actuating mechanisms of the relative rotations of the robotic links and the actual fitting curve, versus the reference body wave in the robotic fish, where $x = 0$ is at a distance 30% along the body length. (b) Schematic view of the robotic mackerel and its inside implementation. (c) Actuation mechanisms of the relative rotations of the robotic links. (d) Snapshot of the robotic fish experimental apparatus.

TABLE I
BODY AND MASS PARAMETERS, WHERE L DENOTES THE FISH LENGTH

Variable	Mackerel	Robotic fish	Difference
Body length L (m)	0.6	0.593	1.1 %
Caudal span ($/L$)	0.24	0.238	0.8 %
Body volume (L^3)	0.0113	0.01125	4.5 %
Wetted area (L^2)	0.401	0.395	2 %
Mass (kg)	2.68	2.79	4.1 %

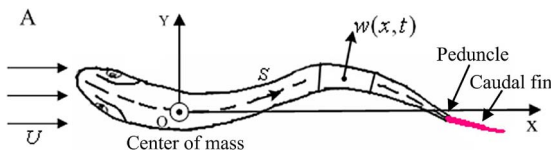

Fig. 3. Sketch of an undulating fish swimming at a self-propelled speed U in x, y global coordinates, where o indicates the fish center of mass, and symbol S denotes the midline along the fish body.

III. KINEMATICS AND DYNAMIC MODELING

Carangiform fish swim in water by propelling themselves, with their body and tail deforming actively, as shown in Fig. 3. One could pose the following question: How does a mackerel resemble an elongated body? In fact, the LAEBT implies that the force produced by a pure body anterior to the caudal fin will not be much different if the body height does not change dramatically [12]. However, the force varies considerably along the caudal fin, i.e., the LAEBT method can be used to evaluate the body-induced thrust force of a carangiform fish by removing the caudal fin. This is also suggested by Hess [18]. In the present dynamic model, the robotic mackerel's caudal fin roughly resembles a triangular foil with an aspect ratio of 2.68. For such flapping foil kinematics, one can employ the unsteady lift theory [15] to evaluate its force production. It should be noted that there is no previous report of an analytical model to solve this problem.

A. Kinematics Modeling of Body and Caudal Fin

The kinematics of the fish body described here has a predetermined time-dependent motion with increasing amplitude from head to peduncle and is assumed to take the form

$$h(x,t) = (c_1 x + c_2 x^2)\sin[kx \pm \omega t], \qquad 0 < x < L - c \quad (1)$$

where $h(x,t)$ denotes the displacement along the lateral direction in a body-fixed coordinate system with x measured from the nose of the robotic fish. c denotes the caudal fin chord length. $k = 2\pi/\lambda$ denotes the wavenumber, corresponding to wavelength λ. $\omega = 2\pi f$ denotes the circular frequency of oscillation. c_1 and c_2 are applied and adjusted to achieve a specific value for the amplitude envelope of the entire fish body. From Fig. 4, the heave and pitch motions of the flapping tail at the pivot point (i.e., the center of mass) are defined as

$$\begin{cases} h_c = [h(x,t)]_{x=L-2c/3} \\ \theta_c = \theta_{\max} \sin\left[\frac{2\pi}{\lambda}x \pm 2\pi f t + \psi\right]_{x=L-2c/3} \end{cases} \quad (2)$$

where h_c and θ_c denote the heave and pitch motions, L represents the fish body length, c denotes the caudal fin chord length, f represents the flapping frequency, $\theta_{\max}$ represents the amplitude of pitch, i.e., slope angle of caudal fin, ψ is the phase

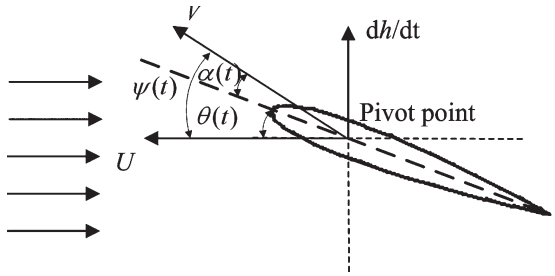

Fig. 4. Definition of relative velocity V and angle of attack $\alpha(t)$ for a flapping tail.

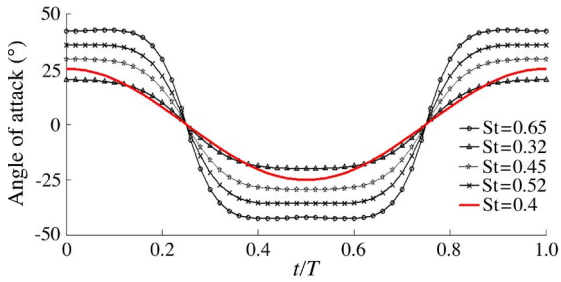

Fig. 5. Angle of attack profiles in an undulating cycle for a fixed maximal slope angle $\theta_{\max} = 25°$, showing the degradation caused by increasing St.

angle between the heave and pitch motions, and $x = L - 2c/3$ denotes the position of the caudal fin pivot point which connects the caudal peduncle.

Fig. 5 shows that the tail's heave motion is aligned with dh_c/dt. The velocity of the incoming flow is perpendicular to the heave motion, and the angle of attack $\alpha(t)$ of the flapping tail is a combination of two factors: the pitch of the tail $\theta_c(t)$ and the heave velocity dh_c/dt. This leads to (3), and considering the kinetic relationship of the body and caudal fin (1)–(3), the angle of attack $\alpha(t)$ can be denoted by (4)

$$\tan\left(\alpha(t) + \theta_c(t)\right) = (dh_c/dt)/U \tag{3}$$

$$a(t) = \left[\arctan\frac{2\pi f h_{\max}\cos\left(\frac{2\pi}{\lambda}x \pm 2\pi f t\right)}{U} - \theta_c \times \sin\left(\frac{2\pi}{\lambda}x \pm 2\pi f t + \psi\right)\right]_{x=L-2c/3}. \tag{4}$$

As the phase angle ψ is set to $\pi/2$, without loss of generality [15], the maximum angle of attack $\alpha_{\max}$ can be expressed by the following:

$$a_{\max} = \arctan\frac{2\pi f h_c}{U} - \theta_{\max}. \tag{5}$$

The Strouhal number [35], which is closely related to the optimal swimming pattern of live swimming fish, is defined as

$$St = \frac{2f|h_c|_{\max}}{U} \tag{6}$$

where $|\cdot|_{\max}$ denotes the maximum value. The distinct angle-of-attack profiles $\alpha(t)$ were investigated previously, and it was found that the cosine wave profile achieved the best thrust performance compared with others [34]. In the conventional robotic fish control method, $\theta_{\max}$ was not varied with St but fixed [24], [37]. To illustrate the disadvantages of this, Fig. 5 shows the angle-of-attack profile for a fixed slope angle $\theta_{\max}$ and varied St. It is obvious that the profiles are very different for low and high St values. For higher St, the maximum angle of attack reaches a value as high as 42°, and the shape of the profile varies considerably with the cosine curve, as shown in Fig. 5. Based on this point, the angle-of-attack profile is set by the following to improve the thrust performance of the flapping tail:

$$a(t) = \left[\alpha_{\max}\cos\left(\frac{2\pi}{\lambda}x \pm 2\pi f t\right)\right]_{x=L-c}. \tag{7}$$

With (5) and (7), the pitch motion of the caudal fin can be given by

$$\theta_c = \left(\arctan\frac{2\pi f h}{U} - \alpha_{\max}\right) \times \cos\left(\frac{2\pi}{\lambda}x \pm 2\pi f t\right)\Big]_{x=L-c}. \tag{8}$$

From the above, the carangiform fish kinematics, which consists of movement of the waving body and flapping tail, has been clearly shown.

B. Body Thrust Modeling

In this section, analytical models that describe a pure body with median fins will be proposed. For a continuous undulating body with swimming speed U, $w(x,t)$ is given by (see Fig. 3 for notation)

$$w(x,t) = \frac{\partial h(x,t)}{\partial t} + U(t)\frac{\partial h(x,t)}{\partial x}. \tag{9}$$

When the fish body is relatively elongated and its cross-sectional area changes slowly along its length, we apply the LAEBT to the fish's undulating body thrust to obtain

$$T_b = \left[m_a w\left(\frac{\partial h}{\partial t} - \frac{1}{2}w\right)\right]_{x=L-c} \tag{10}$$

where T_b denotes the thrust force produced by a pure body and m_a denotes the added mass coefficient per unit length of fish body and is defined as

$$m_a(x) = \frac{1}{4}\beta\rho\pi s(x)^2 \tag{11}$$

where $s(x)$ represents the local height of the fish and ρ represents the water density. For carangiform swimmers, these geometrical features were provided by Videler [23] and can be modeled by

$$s(x) = R_1\sin(R_2 x) + R_3(e^{R_4 x} - 1) \tag{12}$$

where the R_i $(i = 1, 2, \ldots, 4)$ constants can be obtained from [23], and the exact values are presented by following: $R_1 = 0.14L$, $R_2 = 2\pi/1.6L$, $R_3 = 0.0008L$, and $R_4 = 2\pi/1.1L$. The nondimensional virtual mass coefficient β depends on several factors [12]: 1) the fish body cross-sectional shape; 2) a fraction number q of the total depth $s(x)$ occupied by the fish body and the remainder by the dorsal and anal fins; and 3) the ratio of wavelength to the depth of the fish cross section, defined as $\lambda/s(x)$. β_1 can be regarded as the functional result

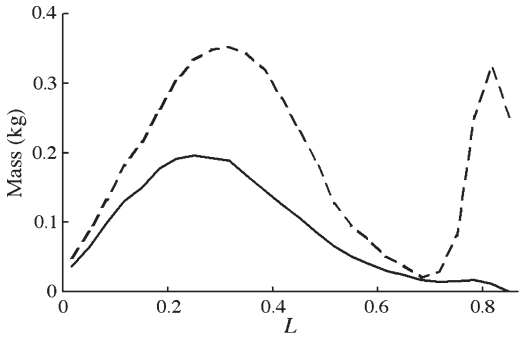

Fig. 6. (Drawn curve) Distribution of body mass per unit length $m(x)$ and (dashed curve) lateral added mass per unit length $m_a(x)$.

of the fish "body shape," and we calculate $\beta_1(x)$ as a function of $q(x)$, as given in (12), by using a third-order approximation with a least squares fit

$$\beta_1(x) = 3 \times 10^{-5} q(x)^3 - 0.0016 q(x)^2 + 0.014 q(x) + 0.966 \tag{13}$$

where the fraction number $q = a/s$, with $s = (a + d + p)$ (see Fig. 1 for notation), where a denotes the main body depth, d denotes the dorsal fin depth, and p represents the pelvic or anal fin depth. $\beta_2(x)$ is relative to the fish kinetic characteristics, which can be approximated by the following:

$$\beta_2(x) = 8 \times 10^{-5} (\lambda/s)^3 - 0.0053(\lambda/s)^2 + 0.1211(\lambda/s) + 0.0769. \tag{14}$$

The dorsal fin geometry function of a carangiform swimmer is obtained from [18], and the aforementioned description enables us to confidently know the virtual mass coefficient per unit length of the fish, including the median fins. Therefore, $\beta(x)$ can be obtained by the following:

$$\beta(x) = \beta_1(x)\beta_2(x). \tag{15}$$

Fig. 6 shows the graphs for the robotic fish body mass distribution and the lateral added mass distribution, which takes the median-fin hydrodynamic effect into account.

C. Caudal Fin Thrust Force Modeling

The hydrodynamic lift force of a flapping tail can be obtained by summing three effects: 1) the quasi-steady lift force due to the angle of attack; 2) the added mass effect of the flapping tail; and 3) the unsteady wake effect induced by the flapping motion. The final expression for the hydrodynamic lift force takes the following form:

$$\begin{aligned} L_c = {} & \pi\rho c U(t)\left(-\dot{h}_c + U\theta_c + \frac{1}{12}c\dot{\theta}_c\right) \\ & + \frac{1}{4}\pi\rho c^2(-\ddot{h}_c + U\dot{\theta}_c - b\ddot{\theta}_c) \\ & - \mathrm{Real}\left(\pi\rho c U(t)\left(-\dot{h}_c + U\theta_c + \frac{1}{12}c\dot{\theta}_c\right)\left(1 - Te\left(\frac{\sigma}{2}\right)\right)\right) \end{aligned} \tag{16}$$

where $\sigma = \omega c/U$ represents the reduced frequency, ω denotes the circular frequency, and $\omega = 2\pi f$. $\mathrm{Real}(\cdot)$ denotes taking the real part, and $Te(\cdot)$ denotes the Theodorsen function, which is defined as

$$\begin{aligned} Te\left(\frac{\sigma}{2}\right) &= \frac{K_1(i\sigma/2)}{K_0(i\sigma/2) + K_1(i\sigma/2)} \\ &= \frac{H_1(\sigma/2)}{H_1^{(2)}(\sigma/2) + iH_0^{(2)}(\sigma/2)}, \qquad \sigma = \frac{\omega c}{U}. \end{aligned} \tag{17}$$

A ratio of third-order polynomials was found to provide good approximation to the Theodorsen function

$$\mathrm{Real}\left(Te\left(\frac{\sigma}{2}\right)\right) = \mathrm{Re}\left(\frac{a_3(i\sigma/2)^3 + a_2(i\sigma/2)^2 + a_1(i\sigma/2) + a_0}{(i\sigma/2)^3 + b_2(i\sigma/2)^2 + b_1(i\sigma/2) + b_0}\right), \quad \sigma = \frac{\omega c}{U} \tag{18}$$

where

$$\begin{aligned} [a_3, a_2, a_1, a_0] &= [0.5, 1.0761, 0.524855, 0.045133] \\ [b_2, b_1, b_0] &= [1.90221, 0.699129, 0.0455035]. \end{aligned}$$

The thrust force produced by the component of the caudal fin lift force acting in the forward direction is given by (19), as there is thrust associated with the leading edge suction, and takes the form of (20)

$$T_{c1}(t) = L_c(t)\sin\theta_c(t) \times S; \tag{19}$$

$$T_{c2}(t) = \pi\rho c S \times \mathrm{Real}\left[\left(-\dot{h}_c + U\theta_c + \frac{1}{12}c\dot{\theta}_c\right)Te\left(\frac{\sigma}{2}\right) - \frac{c}{4}\dot{\theta}_c\right]^2. \tag{20}$$

Therefore, the total thrust force can be simply described as $T_c = T_{c1} + T_{c2}$.

D. Drag Force Modeling

The drag force acting on the anterior rigid head of the robotic fish will take the form

$$F_{dh} = 0.5\rho U^2 C_{fh} S_h + 0.5\rho U^2 C_{dh} A_h \tag{21}$$

where S_h denotes the platform area of the rigid head, A_h denotes the cross-sectional projected area at $x = L/3$, C_{dh} denotes the pressure drag coefficient, and the local viscous drag coefficient C_{fh} is defined as a function of the local axial Reynolds number in a turbulent flow, which is a model based on the classic relationship of a boundary layer on a flat plate [38]

$$C_{fh} = 0.059|\mathrm{Re}^{0.2}| \tag{22}$$

where $\mathrm{Re} = L_h U/\nu$ and L_h denotes the length of a rigid fish head, while at present, $L_h = (1/3)L$. $\nu = 10^{-6}$, which denotes the kinematic viscosity of water. The undulating body drag force is calculated by summing the quasi-steady drag force normal and tangential to the body midline using the undulate kinematics [39], which is integral from the head to the caudal peduncle

$$F_{Db} = \frac{1}{2}\rho \int_0^{L-2c/3} \left[\left(Cd_{x\perp} s(x) \nu_{x\perp}^2\right)\cos\theta + \left(Cd_{x\parallel} s(x) \nu_{x\parallel}^2\right)\sin\theta\right] dx \tag{23}$$

where F_{Db} denotes the drag force of the undulating body. $\nu_{x\perp} = \partial h(x,t)/\partial t$ denotes the fluid velocity normal to the body midline. $\nu_{x\|} = \partial w(x,t)/\partial x$ denotes the fluid velocity tangential to the body. $\theta = \partial h(x,t)/\partial t$ denotes the angle of the local body segment along the x coordinate. The normal and tangential drag coefficients $Cd_{x\perp}$ and $Cd_{x\|}$ are estimated by the empirical description of turbulent flow normal to the cylinder with an ellipse cross section and parallel to a flat plate [38] and can be defined as

$$Cd_{x\perp} = 1.2 + 4\mathrm{Re}_{x\perp}^{-0.5} \qquad \mathrm{Re}_{x\perp} = s(x)\nu_{x\perp}/\upsilon \tag{24}$$

$$Cd_{x\|} = 0.37(\log \mathrm{Re}_{x\|})^{-2.6} \qquad \mathrm{Re}_{x\|} = x\nu_{x\|}/\upsilon \tag{25}$$

where Re denotes the Reynolds number. The drag force for the flapping tail can be described as

$$F_{dc} = \frac{1}{2} C_{dc} \rho U^2 s_c \tag{26}$$

where the unsteady drag coefficient $C_{dc} = 0.063$, the value of which is the result of the experimental data compared with the linear inviscid theory [1]. S_c denotes the caudal fin area, which can be computed as $S_c = 0.5S \times c$.

E. Self-Propelled Swimming Speed and Thrust Efficiency

From the fluid point of view, the self-propelled swimming speed U in a forward direction is determined by the external force exerted on the fish body. The lateral and rotational movements are not obvious when swimming forward. Currently, we only consider the forward direction of the fish swimming with lateral and rotational direction constraints. This simplified method has been widely employed in previous experimental and numerical hydrodynamic research. We do not consider complicated physical factors such as the body–caudal fin interaction [40]. The force balance condition in the forward direction can be described as follows:

$$(T_b + T_c) - (F_{dh} + F_{db} + F_{dc}) = m\frac{dU(t)}{dt}. \tag{27}$$

One can solve the speed $U(t)$ according to (27). When considering the thrust efficiency of the robotic fish, the Froude efficiency η based on the improved form of LAEBT, which takes the slope angle effect into account, has been used to estimate the thrust efficiency of live carangiform swimmers [41]. This is employed for current estimates of thrust efficiency and is given in

$$\eta = \frac{1}{2}(1+\delta) - \frac{1}{2}\gamma^2(\delta^2/1+\delta) \tag{28}$$

where

$$\gamma = \left[\frac{tg\theta_{\max}}{|h(x,t)|_{\max}} \times \frac{\lambda}{2\pi}\right]_{x=L-2c/3} \tag{29}$$

where δ denotes the slip velocity defined as the ratio of the steady swimming speed U to the body wave speed V_b, and $V_b = \lambda f$. $\theta_{\max}$ has been defined in (2), which also represents the slope angle of the caudal fin.

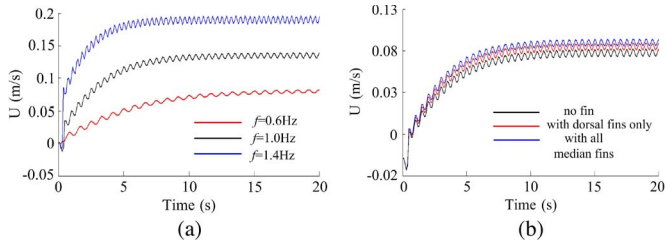

Fig. 7. (a) Time history of the simulation results with kinetic parameters: $\lambda = 0.95$; $f = 0.6, 1.0,$ and 1.4 Hz; $h = 0.1L$; $\alpha_{\max} = 30^\circ$ with median fins. (b) Simulation result of a robotic fish swimming with (1) no fins, (2) a dorsal fin only, and (3) an all-median fin with kinematic parameters: $f = 1.0$ Hz and $h = 0.1$.

IV. Simulation and Experimental Results

To validate the feasibility of the dynamic model and investigate the thrust performance of robotic fish, both simulations and experiments were carried out. It was decided to perform systematic tests at a number of fixed undulating frequencies: $f = 0.4{-}2.2$ Hz with increments of 0.2 Hz. At each value of undulating frequency, the tests were performed for a number of fixed maximum angles of attack, where $\alpha_{\max} = 15^\circ, 20^\circ,$ and 25°. Furthermore, for each combination of f and $\alpha_{\max}$, the dimensionless amplitude was set at $h = 0.075, 0.1,$ and 0.125 in the test, where the dimensionless amplitude h is defined as $h = h_{\max}/L$.

A. Simulation Results and Validations

First, we show the swimming performance of the dynamic simulation result. Fig. 7(a) presents three simulation runs, which show the velocity components of the center of mass for three distinct swimming results in the axial direction over 20 s. As can be seen in the graph, for relatively high flapping frequencies, an initially rapid acceleration can be obtained. After several cycles of undulating movement, the quasi-steady state appears to have been reached, and the amplitude of the oscillations in the steady state represents a departure of $\pm 8\%$. In Fig. 7(b), it can be observed that fish with all median fins consequently reach the highest steady swimming speed relative to the other two cases and fish with no dorsal or anal fins achieve minimal speed than the other two cases.

As can be seen in Fig. 8(a), simulation results show that the final steady swimming speed increases with flapping frequency f; however, it decreases with the maximum angle of attack $\alpha_{\max}$. As can be seen in Fig. 8(b) and (c), the experimental results are somewhat lower than the simulated values due, perhaps, to unknown fluid effects such as surface wave interaction. However, as shown in Fig. 8(d), the simulated speed matches well with the experimental data at $h = 0.125$. Although the current analytical model does not capture every aspect of the fluid effect, according to the experimental validation, the qualitative and quantitative results of the simulation are quite similar to those from the experiments, and the viability of the dynamic model is acceptable. Therefore, the current dynamic model is adequate for further investigation of optimal swimming pattern analysis and control.

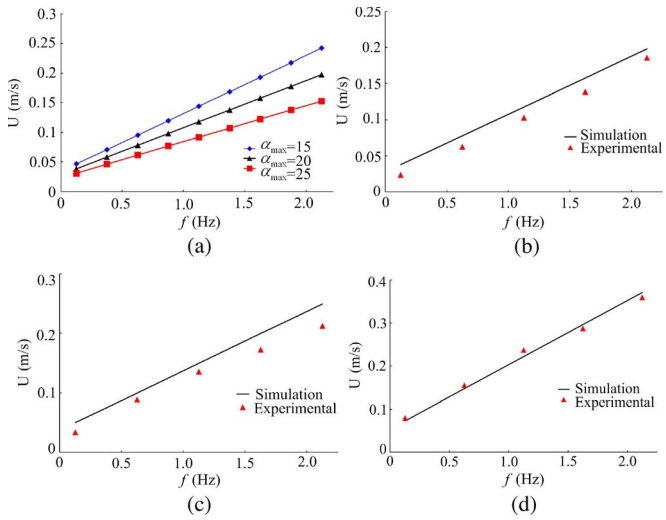

Fig. 8. (a) Frequency versus swimming speed as a function of the maximum angle of attack $\alpha_{\max} = 15°, 20°$, and $25°$ at $h = 0.1$. (b), (c), and (d) show the experimental swimming speed validations for simulation results with kinematics parameters: $f = 1.0$ Hz, $\alpha_{\max} = 20°$, and $h = 0.075$, $h = 0.1$, and $h = 0.125$, respectively.

B. Investigation of Optimal Swimming Pattern

Many studies have shown that fish will tune their kinematics in different surrounding flows to produce an optimal wake for maximum thrust efficiency within a narrow range of St numbers $(0.25 < St < 0.35)$, which can be seen from the shallow area in Fig. 9. For the definition of St, see (6). In this paper, over 80 experiments were conducted. Fig. 9 shows the St under conditions of self-propulsion as a function of the swimming speed U for all simulation runs.

It is evident in Fig. 9(a) that the simulation result for the St number ranges between 0.37 and 0.69 is in good agreement with the experimental result where the St number was within the range of 0.41–0.72 for all parameter sets [34]. The experimental results can be seen in Fig. 9(b). Moreover, the St number shows no tendency to vary with the swimming speed at a fixed angle of attack $\alpha_{\max}$ and a dimensionless amplitude h, which is similar to the observed biological results [1]. With increasing $\alpha_{\max}$, the St number gradually deviates from that of the live fish steady swimming region $(0.25 < St < 0.35$, shadow area). It is obvious that the St number for robotic fish is higher than that for live swimming fish.

We also provide detailed data for the optimal swimming case, where simulation, experiment, and previous estimates of a live swimmer are shown in Table II. It is clear that the simulation results for efficiency are lower than those for a live swimmer using the same method. Cheng [41] reported an efficiency of 89% for a live mackerel. Our experimental results [34] are also somewhat lower than the current simulation results, as can be seen in Table II. It is likely that the LAEBT method overestimates the hydrodynamic forces acting on the undulating body, which is indicated by previous researchers.

By varying the kinematics parameters, the thrust efficiency η of the simulation results for all cases is shown in Fig. 9(c). The general trend of thrust efficiency showed similarities with the observed results of live fish [23]. A maximum efficiency of 67.5% is recorded at $St = 0.398$, $\alpha_{\max} = 15°$, and $h = 0.125$,

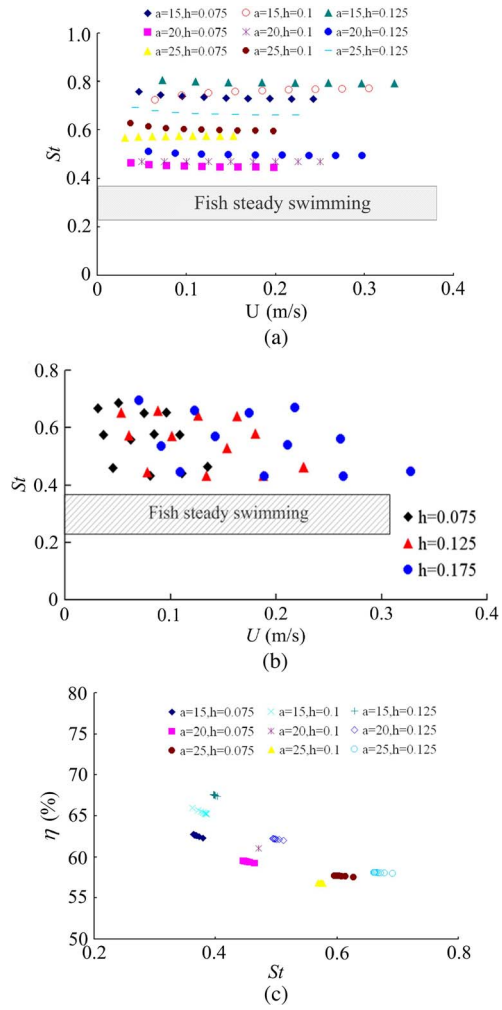

Fig. 9. (a) Simulation results of the swimming St number versus speed U, where a in the figure denotes the angle of attack. (b) Experimental results of the swimming St number versus speed U. (c). Thrust efficiency versus St as a function of the angle of attack.

TABLE II
QUALITATIVE DATA OF SIMULATION AND EXPERIMENTAL RESULTS

Variable	Symbol	Sim	Exp	Live
Body length (m)	L	0.59	0.59	0.4
Flapping frequency	f	0.4–2.0	0.6–1.8	1.0–3.0
Wave length (L)	λ	0.95	0.95	0.95
Tail end amplitude (L)	h	0.1	0.1	0.083
Strouhal number	St	0.398	0.41	0.34
Slope angle	θ_{max}	0.289	0.289	0.3
Froude efficiency	η	67.5 %	61 %	89 %

while at $h = 0.075$, a minimum thrust efficiency of 51.8% is obtained at $St = 0.57$ and $\alpha_{\max} = 20°$. Overall, the thrust efficiency decreases with increasing St and $\alpha_{\max}$, while for a given St, as can be seen in Fig. 9(c), the thrust efficiency increases with h. This also means that, at the same St, better thrust performance can be achieved at a larger h with a relatively lower f, rather than employing a higher f with a lower h. This result agrees well with Read's study on a finite flapping foil [36]. Most fish swim near a "universal" St, which can be denoted as St_{opt}, and $0.25 < St_{\text{opt}} < 0.35$. Experimental

results of a flapping foil also suggested that fish prefer this specific value of St because the swimming efficiency is indeed maximized near $St_{\rm opt}$. On the basis of studying live swimmers, the $St_{\rm opt}$ for robotic fish can also be obtained from the St value at which maximum thrust efficiency is recorded.

The principal results that follow from the aforementioned figures and descriptions can be summarized as follows.

1) Robotic fish with median fins can obtain better swimming performance than that with a "bare" body. It should be noted that this point was ignored in most previous designs of robotic fish.
2) A maximum thrust efficiency (67.5% by simulation and 61% by experiment) is obtained for an St of 0.398, at an $\alpha_{\max}$ of 15°. To obtain higher thrust efficiency, larger $\alpha_{\max}$ should be set for higher St.

The flapping foil [33] achieves the highest efficiency at St numbers in the range 0.3–0.4, associated with angles of attack in the range 15°–25°, which is in good agreement with the results of this study. It is not surprising to find that the maximum thrust efficiency is observed in kinetic parametric values for which a flapping foil is efficient, since the flapping tail produces most of the thrust force while the fish is swimming. Therefore, in this study, the dimensionless parameter $St_{\rm opt}$ is chosen to be 0.398 for the application of the control method, which will be introduced in the following section.

V. Efficient Swimming Control Methods and Results

Implementation and simulation results for swimming speed and thrust efficiency of robotic fish using three distinct control methods, namely, open-loop, conventional PID, and fuzzy logic controllers, will be proposed and compared in this section.

A. Design of Classical PID Controller

First, we outline PID control fundamentals [42], [43]. The conventional PID controllers were applied to robotic fish control. It should be noted that, in previous studies, the control variable is usually the flapping frequency f with the slope angle $\theta_{\max}$ fixed. We recall that, in the investigation of Yu *et al.*, $\theta_{\max} = 20.5°$ [7], and $\theta_{\max} = 30°$ was used by Klein and Morgansen [37]. In the current PID controller, the slope angle $\theta_{\max}$ will be fixed at 25°, and the desired speed will be realized by changing the frequency f. The conventional PID controller in its discrete form can be characterized by

$$\Delta f(k) = k_p e(k) + k_d \Delta e(k) + k_i \sum_{i=0}^{k} e(i), \qquad i = 1, 2 \ldots \quad (30)$$

where k denotes a discrete-time instant and $\Delta f(k)$ indicates the output frequency deviation at a certain instant. k_p, k_i, and k_d are defined to be proportional, integral, and derivative gains. $e(k)$ and $\Delta e(k)$ are the speed error terms at a certain time instant, and $\Delta e(k)$ denotes the acceleration rate of the robotic fish, defined as follows:

$$e(k) = U_d - U_c(k) \qquad \Delta e(k) = e(k) - e(k-1). \quad (31)$$

U_d denotes the desired speed for the robotic fish, and U_c represents the current speed obtained from velocity feedback. A positive value of $e(k)$ means that the robotic fish needs to accelerate to a desired speed at instant k, whereas a negative value of $e(k)$ means that the fish needs to decelerate. The flapping frequency of a robotic fish at certain instant k is

$$f(k) = \Delta f(k) + f(k-1). \quad (32)$$

With (1) and (32), the kinematics of robotic fish can be determined, and with the application of the Newton equation (28), the robotic fish will gradually accelerate to the desired speed.

B. Design of Efficient Swimming Controller

In the discussion on optimal swimming patterns in Section IV, we suggested that efficient swimming of robotic fish does not depend solely on St, but the angle of attack $\alpha_{\max}$ should be actively controlled in association with changing St. The issue is how do we apply this extensive knowledge and experience to the harmonic control of St and $\alpha_{\max}$ to improve the thrust efficiency of robotic fish. Wolfgang *et al.* reported St uncertainties of ∼50% with gentle acceleration in live swimmers [40]. From our studies on natural creatures, we proposed a novel control method which can actively control the Strouhal number St and the caudal fin angle of attack $\alpha_{\max}$.

1) Controller Fundamentals Structure: As can be seen in Fig. 10, the basic structure of the control system consists of the fuzzy controller block, expert controller block, and fish swimming dynamics block. The self-propelled swimming speed $U_c(t)$ is compared with the desired speed U_d to provide the speed error terms. The fuzzy controller decides the Strouhal number deviation ΔSt according to the speed error inputs, and the expert controller is applied to select the proper $\alpha_{\max}$ associated with the St. The fish swimming dynamics will result from the input dimensionless parameters, i.e., St and $\alpha_{\max}$; thus, robotic fish swimming speed is obtained.

2) Design of the Fuzzy Controller: The fuzzy controller can be viewed as an artificial decision maker [44], [45] that operates in the closed-loop speed control of the robotic fish, which is clearly shown by the dashed line box in Fig. 10. Here, a discrete-time controller with two inputs and a single output is considered for the implementation. The inputs $e(k)$ and $\Delta e(k)$ have the same definitions as in (32). The actual range of values of $e(k)$ is between -0.6 and 0.6 m/s, and that of $\Delta e(k)$ is between -0.2 and 0.2 m/s. During the fuzzification stage, $e(k)$ and $\Delta e(k)$ are multiplied by scaling factors: $k_1 = k_2 = 10$. The value of the input variable $e(k)$ is then fuzzified and expressed as E and denoted by the linguist fuzzy sets $\{NB, NS, ZE, PS, PB\}$, abbreviated from *negative big, negative small, zero, positive small,* and *positive big*, respectively. $\Delta e(k)$ is expressed as EC and denoted by $\{N, ZE, P\}$, abbreviated from *negative*, *zero*, and *positive*, respectively.

The actual range of the controller output is $-0.2 < \Delta St < 0.2$, and this range of values is chosen to be nearly 50% of the value of $St_{\rm opt}$, similar to the observed results of a live fish [35]. The output variable is expressed as Lst and denoted by the linguist fuzzy sets $\{NB, NS, ZE, PS, PB\}$,

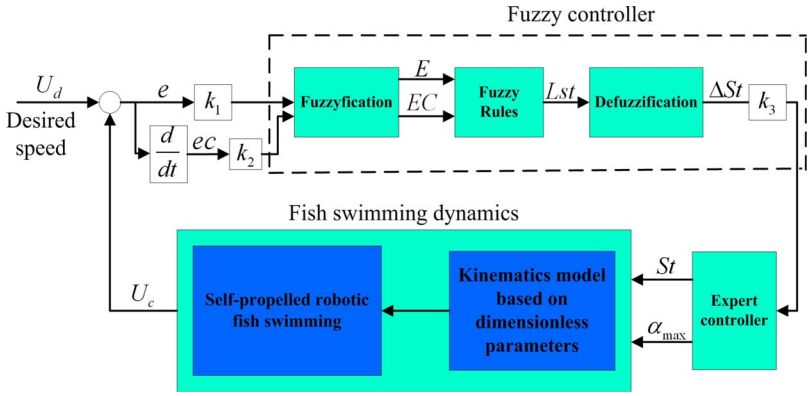

Fig. 10. Controller block for robotic fish.

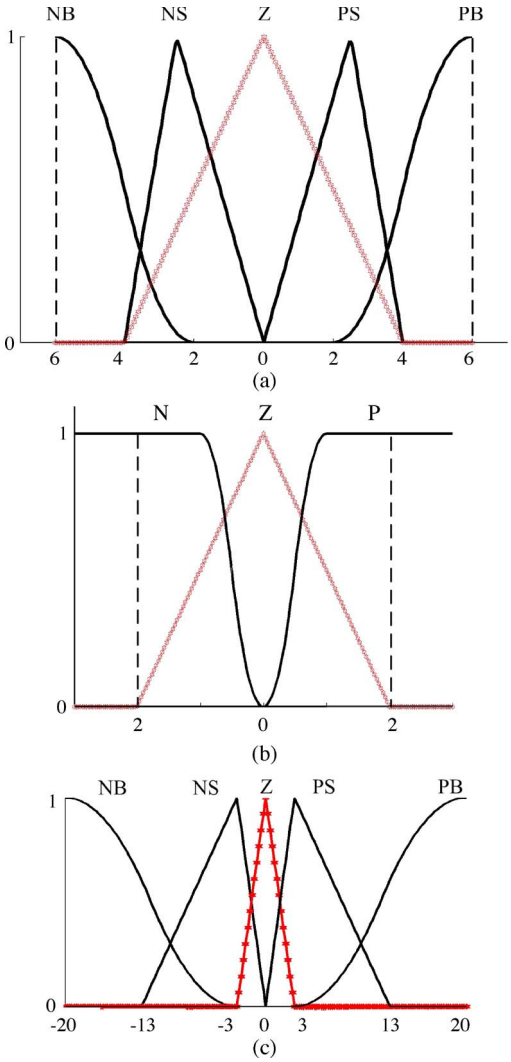

Fig. 11. (a) Membership function of E. (b) Membership function of EC. (c) Membership function of output ΔSt.

denoting *negative big, negative small, zero, positive small,* and *positive big*. The membership functions of the input (i.e., E and EC) and output variable (Lst) are sets of overlapping values represented by Z and triangular- and sigmoid-shaped functions, as shown in Fig. 11.

TABLE III
RULE TABLE FOR FUZZY CONTROLLER

Lst		EC		
		N	Z	P
E	NB	NB	NB	NB
	NS	NS	NS	NB
	Z	PS	Z	NS
	PS	PB	PS	PS
	PB	PB	PB	PS

Fig. 11(a) and (b) shows the sets of membership functions for the speed error inputs, while the output ΔSt, whose membership is shown in Fig. 11(c), will be adjusted according to the inputs. It should be noted that the membership functions are determined by hydrodynamic knowledge and experience. As a simple example, when the membership function of E is within the domain [0, 6] for an actual value of 0–0.6 m/s, the current speed is lower than the desired speed. While for a domain of output variable ΔSt, taking the range [0, 20], the Strouhal number of the robotic fish will increase in order to accelerate.

The following step in the fuzzy controller is to specify the fuzzy rules that can be represented and stored by the fuzzy associative memory (FAM) matrix. A 2-D (5×3) FAM matrix is given in Table III, where the fuzzy rules are described using fuzzy linguistics which comprises the IF–THEN statement such as:

$$\{\text{If } E \text{ is } PB \text{ and } EC \text{ is P, then } Lst \text{ is } PS\}.$$

This fuzzy logic set can be interpreted as follows:

{when the difference between the desired speed and the current speed of the robotic fish E is positive and large, while the fish's forward acceleration EC is positive, then the robotic fish needs a small increment of St to accelerate to the desired speed U_d.}

In general, the IF-THEN statement is actually as follows: {If E is E_i and EC is EC_j, then Lst is Lst_{ij}}, where the subscripts i and j denote the ith and jth of fuzzy sets E and EC, respectively.

During the stage of defuzzification, we adopt the Mamdani fuzzy inference method, and the precise values of the output

variables are determined using the center-of-gravity defuzzification method

$$\Delta St = \frac{\sum_{k=1}^{15} u_{ij} Lst_{ij}}{\sum_{k=1}^{15} u_{ij}} \tag{33}$$

where u_{ij} is the weight factor, which is obtained by Mamdani inference with minimum for intersection and maximum for union, at a certain instant k; the weight factor can be expressed by the following:

$$u_{ij} = \min\left(E_i\left(e(k)\right), EC_i\left(\Delta e(k)\right)\right). \tag{34}$$

In addition, as shown in Fig. 10, the output value of ΔSt will be multiplied by the scaling factors: $k_3 = 0.01$. Consequently, at a certain instant k, the Strouhal number can be obtained

$$St(k) = St_{\text{opt}} + \Delta St(k) \tag{35}$$

where St_{opt} denotes the optimal value of the Strouhal number and is set at 0.398, as indicated in Section IV. The efficient propulsion of robotic fish can only be achieved by adopting a harmonic combination of St and $\alpha_{\max}$, as indicated previously. The purpose of the expert controller is to choose the appropriate maximum angle of attack for different Strouhal numbers at certain instants. Piecewise, in terms of the distribution function, the expert controller is given by the following:

$$\alpha_{\max} = \begin{cases} 15^\circ (0.2 < St \leq 0.35) \\ 20^\circ (0.35 < St \leq 0.45) \\ 25^\circ (0.45 < St \leq 0.6). \end{cases} \tag{36}$$

3) Swimming Dynamics Based on Dimensionless Parameters: With (6), the flapping frequency f can be denoted as a function of St

$$f = \frac{St \times U}{2h_{\max}}. \tag{37}$$

From (1), (35), and (37), the discrete form of the body kinematics model based on dimensionless parameters (see Fig. 10 for notation) at instant k can be expressed as

$$h(x,k) = (c_1 x + c_2 x^2) \times \sin\left[\frac{2\pi}{\lambda}x + \frac{\pi\left(St_{\text{opt}} + \Delta St(k)\right) \times U}{h_{\max}}k\right], \quad 0 \leq x \leq L - c. \tag{38}$$

The caudal fin pitch motion $\theta_c(k)$ is then presented as

$$\theta_c(k) = \left(\arctan\left[\pi St(k) - \alpha_{\max}(k)\right] \times \cos\left(\frac{2\pi}{\lambda}x + \frac{\pi St(k) \times U(k)}{h_{\max}}k\right)\right), \quad x = L - 2c/3. \tag{39}$$

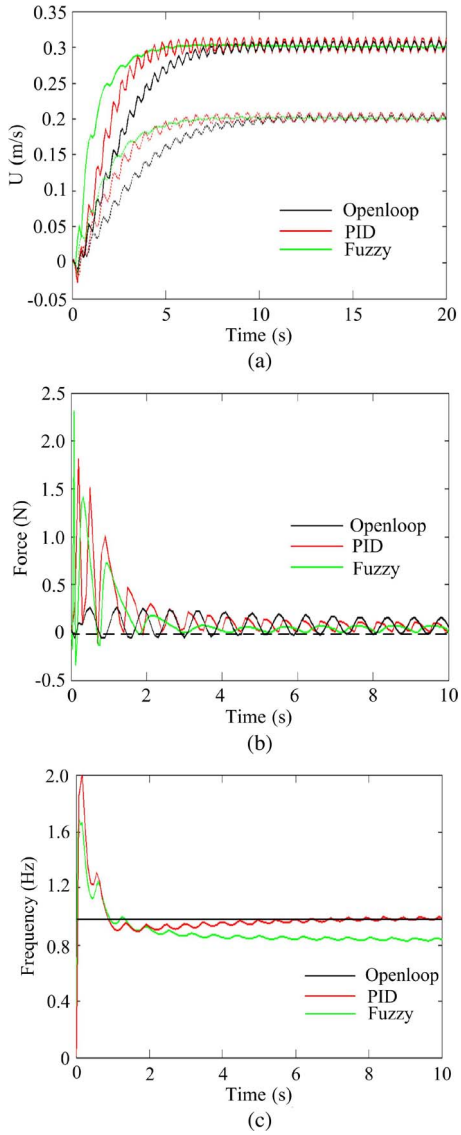

Fig. 12. (a) Simulation speed for the desired speed U_d of (dashed curve) 0.2 and (drawn curve) 0.3 m/s. (b) Time history of the caudal fin thrust force T_c in 10 s for $U_d = 0.2$ m/s, where the dashed line indicates zero force. (c) Simulation time history of the flapping frequency f in 10 s for $U_d = 0.2$ m/s.

Substituting the kinematics (38) and (39) into the dynamic (27), we can solve the swimming speed U of the robotic fish. The whole control process was implemented in Matlab.

C. Simulation Results

The simulation results of both the speed response and thrust efficiency using the open-loop, PID, and fuzzy controllers are evaluated and compared in this section. The dimensionless amplitude h was fixed to 0.1 for all three methods, and the parameters for the PID controller are $k_p = 0.2$, $k_i = 0.01$, and $k_d = 5$. The flapping frequency can be controlled via (31) and (33). The caudal fin slope angle $\theta_{\max}$ is fixed at 25° for both the PID and open-loop controllers.

1) Swimming Speed: Fig. 12(a) shows the velocity component of the robotic fish in the forward direction over 20 s of body movement. The robot is given two distinct desired speeds

TABLE IV
COMPARISON OF FUZZY CONTROL METHOD VERSUS PID AND OPEN-LOOP CONTROL METHODS FOR $U_d = 0.2$ m/s

Performance Specification	Open-loop	PID	Fuzzy
Settling time (s)	10.5	6.5	6.0
Rising time (s)	6.5	4.2	3.6
Steady-State Error (%)	8.5	6.6	2.2
Thrust efficiency (%)	60.2	60.2	69.4
Strouhal number	0.58	0.58	0.401

(U_d) of 0.2 and 0.3 m/s. The PID and fuzzy controllers show good tracking performances with the desired speed. During the initial start phase, the speed under closed-loop control is seen to accelerate faster than that of the open-loop control [see Fig. 12(a) for details]. The settling times at an input speed of 0.3 m/s are 6.5 s for the PID controller and 6 s for the fuzzy controller, while the rise times are 4.2 s for the PID controller and 3.6 s for the fuzzy controller. However, open-loop swimming performance lags far behind the performance of closed-loop methods, as can be seen in Table III, which provides the qualitative results of the speed response. It should be noted that, due to the large damping effect of water, almost no overshoot was observed for both the PID and fuzzy controllers. Similar phenomena were also reported by Klein and Morgansen [37], who applied the PID control method to robotic fish.

With regard to the steady-state error (SSE), all three methods performed speed oscillations. This is in accordance with the biologists' observed results for live fish [3]. See Fig. 12(a) and Table III for details. The robotic fish using the fuzzy control method performed the smoothest speed trace, with an SSE of about 2.2% during steady swimming. The PID controller had obviously larger SSE of about 6.6%, while the open-loop method produced the largest speed fluctuations with an SSE of 8.5%. The cause of the SSE is the force oscillations within a flapping cycle. The robotic fish caudal fin thrust force T_c, which is derived from (21) and (22), would give rise to the speed as well as produce the SSE, as shown in Fig. 12(b). Under fuzzy control, robotic fish produced the largest caudal fin thrust force among all three methods over the initial 2–3 s, and the acceleration capability corresponding to this force is also reflected in the forward speed, which can be seen in Fig. 12(a). However, a very interesting finding can be observed in Fig. 12(b), which is that, after 5 s from the initial start, the thrust force under fuzzy control method becomes smoother than those under PID and open-loop control methods. As was suggested in previous studies on the flapping foil [36], the caudal fin angle of attack when not actively controlled will produce a larger unsteady force, which is caused by the influence of the discrete shedding vortices and the ill-defined wake topology. This is also the main cause for the larger force and speed fluctuations of PID control and open-loop methods.

2) Thrust Efficiency: Taking into account the thrust efficiency reported in Table IV, and as shown in Fig. 12(c), the most important findings are as follows: 1) A robotic fish with fuzzy control swims more efficiently than that with the open-loop and PID controllers, and 2) in a steady swimming state, a smaller flapping frequency f is needed using the fuzzy controller compared with other two methods. As can be seen from Fig. 12(c), in the initial 2 s, both the PID and fuzzy control methods employed a relatively high flapping frequency. After several circles which take about 5 s, the frequencies for these two methods become unequal. The frequency for the PID controller appears to gradually increase and reach a constant value (where $f = 1.05$ Hz), which is quite close to the open-loop frequency. However, different trends were observed for the fuzzy controller situation, where the frequency f ultimately decreased to a lower constant value ($f = 0.81$ Hz). This behavior is the result of proper control of the caudal fin movement using the fuzzy control method. The robotic fish can achieve the desired speed by adopting a lower frequency. With the definition of the thrust efficiency η expressed in (28), it is not difficult to establish why a higher η can be obtained using the present method.

In Table IV, it can be observed that the robotic fish with fuzzy control had lower St than the other two methods ($St = 0.401$), which is close to the regime of live swimmers ($0.25 < St < 0.35$). According to (35), we see that St via the present fuzzy method is controlled within a certain range; therefore, we can speculate that the robotic fish has similar swimming characteristics to natural creatures, which can always swim near their own "universal" optimal Strouhal number. Although the fuzzy control method presented here shows the feasibility for speed tracking, as well as maintaining relatively high thrust efficiency for robotic fish, this method is based entirely on nature.

VI. RESULTS

This paper has proposed a dynamic model of a carangiform robotic fish, which treats the force of the undulating body and caudal fin independently. The simulation speed results are validated through comparison with experimental results. The results demonstrated that robotic fish with median fins obtained a better thrust performance than those with no median fins. Based on the present dynamic model, harmonic control of the Strouhal number and caudal fin angle of attack proved to be a principal mechanism through which robotic fish achieve high thrust efficiency. This is also the most important reason why the fuzzy control method, which was successfully applied to this principal mechanism, offered better swimming performance and higher thrust efficiency than the conventional PID and open-loop controllers.

Unlike the insect fly which is inherently unstable and must stabilize its flight by frequently adjusting its control variables [46] from the point of view of biomimetic fluid mechanics, due to the large damping effect of water, the swimming speed of the fish is much easier to control and achieves a stable mode in steady flow without disturbance. This point was also suggested by biologists' studies. However, a very interesting topic arises, which is as follows: What type of control system should be proposed to maintain stability if there are external perturbations, such as vortices and waves? Research on the stability of live fish in perturbation environments is still in its infancy [47]. A great deal of work remains to be done, particularly in the development of intelligent control systems [48], [49] for the stability of robotic fish in disturbed flow. This is one of our future research priorities.

ACKNOWLEDGMENT

The authors would like to thank Prof. G. V. Lauder for his kind suggestions on this research.

REFERENCES

[1] M. S. Triantafyllou, G. S. Triantafyllou, and D. K. P. Yue, "Hydrodynamics of fish swimming," *Annu. Rev. Fluid Mech.*, vol. 32, pp. 33–53, 2000.
[2] M. H. Dickinson, F.-O. Lehmann, and S. P. Sane, "Wing rotation and the aerodynamic basis of insect flight," *Science*, vol. 284, no. 5422, pp. 1954–1960, Jun. 1999.
[3] E. D. Tytell, "Do trout swim better than eels? Challenges for estimating performance based on the wake of self-propelled bodies," *Exp. Fluids*, vol. 43, no. 5, pp. 701–712, 2007.
[4] T. Wang, L. Wen, J. Liang, and G. Wu, "Fuzzy vorticity control of a biomimetic robotic fish using a flapping lunate tail," *J. Bionic Eng.*, vol. 7, no. 1, pp. 56–65, Mar. 2010.
[5] W. Li, T. Wang, L. Jianhong, and L. Jinlan, "Fuzzy logic vorticity control of oscillating foil UUV," in *Proc. IEEE/RSJ Int. Conf. Intell. Robots Syst.*, 2009, pp. 1019–1024.
[6] M. Sfakiotakis, D. M. Lane, and J. B. C. Davies, "Review of fish swimming modes for aquatic locomotion," *IEEE J. Ocean. Eng.*, vol. 24, no. 2, pp. 237–252, Apr. 1999.
[7] J. Yu, M. Tan, S. Wang, and E. Chen, "Development of a biomimetics robotic fish and its control algorithm," *IEEE Trans. Syst., Man, Cybern. B, Cybern.*, vol. 34, no. 4, pp. 1798–1810, Aug. 2004.
[8] Y. Hu, W. Zhao, and L. Wang, "Vision-based target tracking and collision avoidance for two autonomous robotic fish," *IEEE Trans. Ind. Electron.*, vol. 56, no. 5, pp. 1401–1410, May 2009.
[9] F. E. Fish and G. V. Lauder, "Passive and active flow control by swimming fishes and mammals," *Annu. Rev. Fluid. Mech.*, vol. 38, no. 1, pp. 193–224, 2006.
[10] U. K. Muller, B. Van den Heuvel, E. J. Stamhuis, and J. J. Videler, "Fish foot prints: Morphology and energetics of the wake behind a continuously swimming mullet (*Chelon labrosus* Risso)," *J. Exp. Biol.*, vol. 200, no. 22, pp. 2893–2906, Nov. 1997.
[11] U. K. Muller, E. J. Stamhuis, and J. J. Videler, "Hydrodynamics of unsteady fish swimming and the effects of body size: Comparing the flow fields of fish larvae and adults," *J. Exp. Biol*, vol. 203, no. 2, pp. 193–206, Jan. 2000.
[12] M. J. Lighthill, "Aquatic animal propulsion of high hydrodynamic efficiency," *J. Fluid Mech.*, vol. 44, pp. 265–301, 1970.
[13] K. A. McIsaac and J. P. Ostrowski, "Motion planning for anguilliform locomotion," *IEEE Trans. Robot. Autom.*, vol. 19, no. 4, pp. 637–652, Aug. 2003.
[14] F. Boyer, M. Porez, A. Leroyer, and M. Visonneau, "Fast dynamics of an eel-like robot—Comparisons with Navier–Stokes simulations," *IEEE Trans. Robot.*, vol. 24, no. 6, pp. 1274–1288, Dec. 2008.
[15] K. Streitlien and G. S. Triantafyllou, "On thrust estimates for flapping foils," *J. Fluids Struct.*, vol. 12, no. 1, pp. 47–55, Jan. 1998.
[16] K. A. Harper, M. D. Berkemeier, and S. Grace, "Modeling the dynamics of spring-driven oscillating-foil propulsion," *IEEE J. Ocean. Eng.*, vol. 23, no. 3, pp. 285–296, Jul. 1998.
[17] K. Morgansen, V. Duindam, R. Mason, J. Burdick, and R. Murray, "Nonlinear control methods for planar carangiform robot fish locomotion," in *Proc. IEEE Int. Conf. Robot. Autom.*, 2001, pp. 427–434.
[18] F. Hess and J. J. Videler, "Fast continuous swimming of saithe (*Pollachius virens*): A dynamic analysis of bending moments and muscle power," *J. Exp. Biol.*, vol. 109, no. 1, pp. 229–251, Mar. 1984.
[19] H. Hu, J. Liu, I. Dukes, and G. Francis, "Design of 3D swim patterns for autonomous robotic fish," in *Proc. IEEE/RSJ Int. Conf. Intell. Robots Syst.*, 2006, pp. 2406–2411.
[20] J. H. Long, T. J. Koob, K. Irving, K. Combie, V. Engel, N. Livingston, A. Lammert, and J. Schumacher, "Biomimetic evolutionary analysis: Testing the adaptive value of vertebrate tail stiffness in autonomous swimming robots," *J. Exp. Biol.*, vol. 209, pp. 4732–4746, 2006.
[21] J. M. Anderson and N. Chhabra, "Maneuvering and stability performance of a robotic tuna," *Integr. Comp. Biol*, vol. 42, no. 1, pp. 118–126, Feb. 2002.
[22] L. Wen, T. Wang, J. Liang, and G. Wu, "A novel method for simultaneous measurement of internal and external hydrodynamic force of self-propelled robotic fish," in *Proc. IEEE/RSJ Int. Conf. Intell. Robots Syst.*, 2010, pp. 952–957.
[23] J. J. Videler, *Fish Swimming*. London, U.K.: Chapman & Hall, 1993.
[24] J. Yu and L. Wang, "Parameter optimization of simplified propulsive model for biomimetic robot fish," in *Proc. IEEE Int. Conf. Robot. Autom.*, Barcelona, Spain, Apr. 2005, pp. 3317–3322.
[25] J. Liu and H. Hu, "Biological inspiration: From carangiform fish to multi-joint robotic fish," *J. Bionic Eng.*, vol. 7, no. 1, pp. 35–48, Mar. 2010.
[26] W. Zhao, Y. Hu, L. Zhang, and L. Wang, "Design and CPG-based control of biomimetic robotic fish," *IET Control Theory Appl.*, vol. 3, no. 3, pp. 281–293, Mar. 2009.
[27] Z. Chen, S. Shatara, and X. Tan, "Modeling of biomimetic robotic fish propelled by an ionic polymer–metal composite caudal fin," *IEEE/ASME Trans. Mechatronics*, vol. 15, no. 3, pp. 448–459, Jun. 2010.
[28] S. Saimek and P. Y. Li, "Motion planning and control of a swimming machine," *Int. J. Robot. Res.*, vol. 23, no. 1, pp. 27–54, Jan. 2004.
[29] L. Guo, J. Y. Hung, and R. M. Nelms, "Evaluation of DSP-based PID and fuzzy controllers for DC–DC converters," *IEEE Trans. Ind. Electron.*, vol. 56, no. 6, pp. 2237–2248, Jun. 2009.
[30] J. Wang, C. Fu, and Y. Zhang, "SVC control system based on instantaneous reactive power theory and fuzzy PID," *IEEE Trans. Ind. Electron.*, vol. 55, no. 4, pp. 1658–1665, Apr. 2008.
[31] H. Liu, "A fuzzy qualitative framework for connecting robot qualitative and quantitative representations," *IEEE Trans. Fuzzy Syst.*, vol. 16, no. 6, pp. 1522–1530, Dec. 2008.
[32] L. Cai, A. B. Rad, and W.-L. Chan, "An intelligent longitudinal controller for application in semiautonomous vehicles," *IEEE Trans. Ind. Electron.*, vol. 57, no. 4, pp. 1487–1497, Apr. 2010.
[33] N. Kato, "Control performance in the horizontal plane of a fish robot with mechanical pectoral fins," *IEEE J. Ocean. Eng.*, vol. 25, no. 1, pp. 121–129, Jan. 2000.
[34] L. Wen, J. Liang, G. Wu, and J. Li, "Hydrodynamic experimental investigation on efficient swimming of robotic fish using self-propelled method," *Int. J. Offshore Polar Eng.*, vol. 20, no. 3, pp. 167–174, Sep. 2010.
[35] J. M. Anderson, K. Streitlien, D. S. Barrett, and M. S. Triantafyllou, "Oscillating foils of high propulsive efficiency," *J. Fluid Mech.*, vol. 360, pp. 41–72, 1998.
[36] D. A. Read, F. S. Hover, and M. S. Triantafyllou, "Forces on oscillating foils for propulsion and maneuvering," *J. Fluids Struct.*, vol. 17, no. 1, pp. 163–183, Jan. 2003.
[37] D. Klein and K. Morgansen, "Controlled collective motion for trajectory tracking," in *Proc. Amer. Control Conf.*, 2006, pp. 5269–5275.
[38] S. F. Hoerner, *Fluid-Dynamic Lift*. Vancouver, WA: Hoerner Fluid Dynamics, 1985.
[39] C. E. Jordan, "A model of rapid-start swimming at intermediate Reynolds number: Undulatory locomotion in the chaetognath Sagitta elegans," *J. Exp. Biol*, vol. 163, no. 1, pp. 119–137, Feb. 1992.
[40] M. J. Wolfgang, J. M. Anderson, M. A. Grosenbaugh, D. K. Yue, and M. S. Triantafyllou, "Near-body flow dynamics in swimming fish," *J. Exp. Biol.*, vol. 202, no. 17, pp. 2303–2327, Sep. 1999.
[41] J.-Y. Cheng, "Note on the calculation of propeller efficiency using elongated body theory," *J. Exp. Biol.*, vol. 192, no. 1, pp. 169–177, Jul. 1994.
[42] S. Skoczowski, S. Domek, K. Pietrusewicz, and B. Broel-Plater, "A method for improving the robustness of PID control," *IEEE Trans. Ind. Electron.*, vol. 52, no. 6, pp. 1669–1676, Dec. 2005.
[43] S. Tzafestas and N. P. Papanikolopoulos, "Incremental fuzzy expert PID control," *IEEE Trans. Ind. Electron.*, vol. 37, no. 5, pp. 365–371, Oct. 1990.
[44] J. T. Teeter and M.-Y. Chow, "A novel fuzzy friction compensation approach to improve the performance of a DC motor control system," *IEEE Trans. Ind. Electron.*, vol. 43, no. 1, pp. 113–120, Feb. 1996.
[45] Y.-S. Huang, "Function-based controller for linear motor control systems," *IEEE Trans. Ind. Electron.*, vol. 57, no. 3, pp. 1096–1105, Mar. 2010.
[46] M. Sun and J. K. Wang, "Flight stabilization control of a hovering model insect," *J. Exp. Biol.*, vol. 210, no. 15, pp. 2714–2722, Aug. 2007.
[47] A. Przybilla, "Entraining in trout: A behavioral and hydrodynamic analysis," *J. Exp. Biol.*, vol. 213, no. 17, pp. 2976–2986, Sep. 2010, to be published.
[48] S. H. Kim, C. Park, and F. Harashima, "A self-organized fuzzy controller for wheeled mobile robot using an evolutionary algorithm," *IEEE Trans. Ind. Electron.*, vol. 48, no. 2, pp. 467–474, Apr. 2001.
[49] M. A. Fnaiech, F. Betin, G.-A. Capolino, and F. Fnaiech, "Fuzzy logic and sliding-mode controls applied to six-phase induction machine with open phases," *IEEE Trans. Ind. Electron.*, vol. 57, no. 1, pp. 354–364, Jan. 2010.

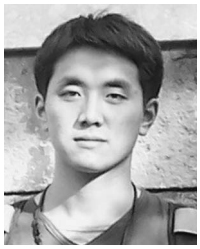

Li Wen received the B.S. degree in mechanical engineering from Beijing Institute of Technology, Beijing, China, in 2005 and the Ph.D. degree from the Department of Mechanical Engineering and Automation, Beihang University, Beijing, in 2011.

He is currently a Postdoctoral Researcher with the Department of Organismic and Evolutionary Biology, Harvard University, Cambridge, MA. Meanwhile, he participated in and served as the Session Chair for several academic conferences, including the IEEE/RSJ International Conference on Intelligent Robots and Systems and IEEE International Conference on Robotics and Automation. His current research interests include biological robotics, experimental fluid mechanics, smart material, and biomechanics.

Dr. Wen was the recipient of many research scholarships during his Ph.D. career and the Best Student Conference Paper award from International Society of Offshore and Polar Engineers Conference in 2010.

Tianmiao Wang received the B.S. degree from X'ian Jiaotong University, Xi'an, China, and the M.S and Ph.D. degrees from Northwestern Polytechnic University, Xi'an, China in 1982 and 1990, respectively.

He is currently the Dean and a Professor with the School of Mechanical Engineering and Automation, Beihang University, Beijing. He is the Head of the Expertized Group in the field of advanced manufacturing technology of the National High Technology Research and Development Program (863 Hi-Tech Program). He has undertaken and finished many national research projects in recent years. He had published nearly 87 papers in local and international journals and three professional books. His research interests include biomimetic robotics, medical robotic technology, and embedded intelligent control technology.

Dr. Wang is a member of China Robotics Society.

Guanhao Wu received the B.S. degree in measurement and control technology and instrumentation program and the Ph.D. degree in optical engineering from Tsinghua University, Beijing, China, in 2003 and 2008, respectively.

He is currently an Assistant Professor with the Department of Precision Instruments and Mechanology, Tsinghua University, Beijing. His research interests include bionic study of fish and insects, and light detection and ranging. He is the author/coauthor of more than ten refereed journal articles and about ten conference papers. He is the holder of six Chinese patents.

Jianhong Liang received the B.S. (in 1999) and Ph.D. degrees in mechanical engineering and automation from Beihang University, Beijing, China.

He is currently an Assistant Professor with the School of Mechanical Engineering and Automation, Beihang University. He had published nearly 40 papers in local and international journals and two professional books. His research interests include biomimetic underwater robotics, field robotics, and small unmanned robotic system.

Dr. Liang was the recipient of many awards.

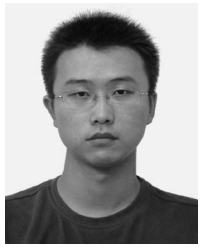

Chaolei Wang received the B.S. degree in mechanical engineering and automation from Beihang University, Beijing, China, in 2004, where he is currently working toward the Ph.D. degree in mechanical engineering and automation.

He is a member of the Laboratory of Intelligent Technology and Robotics, Institute of Robotics, School of Mechanical Engineering and Automation, Beihang University. His research interests are mainly in modeling, identification, control, navigation, and computer vision in small unmanned aerial vehicle.